Chemosphere 299 (2022) 134472

Contents lists available at ScienceDirect

Chemosphere

journal homepage: www.elsevier.com/locate/chemosphere

Laboratory study of iron isotope fractionation during dissolution of mineral dust and industrial ash in simulated cloud water

Elena C. Maters [a,1], Daniel S. Mulholland [b], Pascal Flament [a,*], Jeroen de Jong [c], Nadine Mattielli [c], Karine Deboudt [a], Guillaume Dhont [a], Eugène Bychkov [a]

[a] Laboratoire de Physico-Chimie de l'Atmosphère, Université du Littoral Côte d'Opale, 189A Avenue Maurice Schumann, 59140, Dunkerque, France
[b] Laboratório de Águas e Efluentes & Laboratório de Análises Ambientais, Universidade Federal do Tocantins, Rua Badejos, Gurupi, TO, Brazil
[c] Laboratoire G-Time (Geochemistry: Tracing with Isotope, Mineral and Element), Université Libre de Bruxelles, Avenue Franklin Roosevelt 50, 1050, Brussels, Belgium

HIGHLIGHTS

- Fe solubility and isotopic fractionation of dust and ash are investigated during simulated atmospheric processing.
- The Fe solubility is 40 times higher in the ash than in the dust.
- An isotope fractionation is observed, with preferential release of soluble ^{54}Fe, to a greater extent for the dust than ash.
- Re-adsorption of Fe-oxalate complexes compete with the release of soluble Fe, which maintain a ^{54}Fe enrichment in solution.

GRAPHICAL ABSTRACT

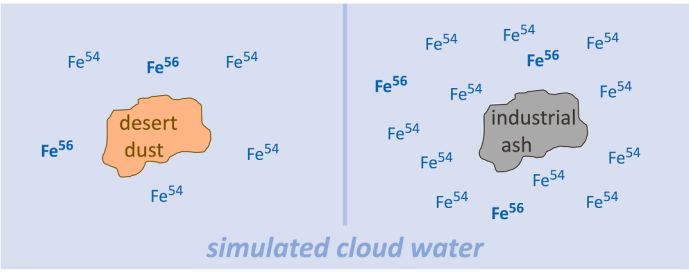

ARTICLE INFO

Handling Editor: R Ebinghaus

Keywords:
Iron isotope
Iron dissolution
Mineral dust
Industrial ash
Atmospheric processing
Isotope fractionation

ABSTRACT

Atmospheric deposition is a key mode of iron (Fe) input to ocean regions where low concentrations of this micronutrient limit marine primary production. Various natural particles (e.g., mineral dust, volcanic ash) and anthropogenic particles (e.g., from industrial processes, biomass burning) can deliver Fe to the ocean, and assessment of their relative importance in supplying Fe to seawater requires knowledge of both their deposition flux and their Fe solubility (a proxy for Fe bioavailability). Iron isotope (^{54}Fe, ^{56}Fe, ^{57}Fe, ^{58}Fe) analysis is a potential tool for tracing natural and anthropogenic Fe inputs to the ocean. However, it remains uncertain how the distinct Fe isotopic signatures (δ^{56}Fe) of these particles may be modified by physicochemical processes (e.g., acidification, photochemistry, condensation-evaporation cycles) that are known to enhance Fe solubility during atmospheric transport. In this experimental study, we measure changes over time in both Fe solubility and δ^{56}Fe of a Tunisian soil dust and an Fe–Mn alloy factory industrial ash exposed under irradiation to a pH 2 solution containing oxalic acid, the most widespread organic complexing agent in cloud- and rainwater. The Fe released per unit surface area of the ash (~1460 μg Fe m^{-2}) is ~40 times higher than that released by the dust after 60 min in solution. Isotopic fractionation is also observed, to a greater extent in the dust than the ash, in parallel with dissolution of the solid particles and driven by preferential release of ^{54}Fe into solution. After the initial release of ^{54}Fe, the re-adsorption of A-type Fe-oxalate ternary complexes on the most stable surface sites of the solid particles seems to impair the release of the heavier Fe isotopes, maintaining a relative enrichment in the

* Corresponding author. Laboratoire de Physico-Chimie de l'Atmosphère, Université du Littoral Côte d'Opale, Bâtiment MREI 2, 189A Avenue Maurice Schumann, 59140, Dunkerque, France.
E-mail address: pascal.flament@univ-littoral.fr (P. Flament).
[1] Now at: Department of Chemistry, University of Cambridge, Lensfield Rd, Cambridge CB2 1 EW, United Kingdom.

https://doi.org/10.1016/j.chemosphere.2022.134472
Received 28 December 2021; Received in revised form 23 March 2022; Accepted 28 March 2022
Available online 31 March 2022

light Fe isotope in solution over time. These findings provide new insights on Fe mobilisation and isotopic fractionation in mineral dust and industrial ash during atmospheric processing, with potential implications for ultimately improving the tracing of natural versus anthropogenic contributions of soluble Fe to the ocean.

1. Introduction

Iron (Fe) plays an important role in many environmental processes, including marine primary production, and thereby affects the global carbon cycle (Boyd and Ellwood, 2010; Tagliabue et al., 2017). Specifically, Fe is an essential micronutrient for marine phytoplankton, and low dissolved Fe concentrations in seawater limit primary production in >30% of the surface ocean (de Baar, 2005; Hutchins and Bruland, 1998; Martin and Fitzwater, 1988; Morel et al., 1991). Iron sources to these so-called High Nutrient Low Chlorophyll (HNLC) ocean regions include inputs from atmospheric deposition, continental margin sediments and hydrothermal vents (Conway and John, 2014; Duce and Tindale, 1991; Lam and Bishop, 2008; Tagliabue et al., 2010). With the increase in human activity, anthropogenic aerosols such as particles from biomass burning, industry and traffic are now also recognised as potential Fe fertilisers (Chen et al., 2020; Ito et al., 2019; Kurisu et al., 2021; Luo et al., 2008; Rodríguez et al., 2021; Sedwick et al., 2007; Shi et al., 2012; Sholkovitz et al., 2009; Wang et al., 2017). Mineral dust from arid and semi-arid regions and particles from fossil fuel combustion may collectively contribute ~50% of the soluble Fe supply to much of the Northern Hemisphere oceans (Ito and Shi, 2016). According to (Ito et al., 2021), pyrogenic particles represent ~20% of the soluble Fe reaching the global ocean surface. However, large uncertainties remain regarding the deposition fluxes and Fe solubilities of these natural and anthropogenic particles (Baker et al., 2016; Mahowald et al., 2009), preventing accurate assessment of their relative importance in influencing surface ocean Fe biogeochemistry. While mineral dust is often considered the primary source of atmospheric Fe to the ocean, anthropogenic particles typically display an Fe solubility orders of magnitude higher than that of dust (<1 wt%) (Luo et al., 2008; Sedwick et al., 2007; Sholkovitz et al., 2012; Takahashi et al., 2013).

Iron isotopes have emerged as a powerful tool for tracing natural and anthropogenic Fe sources in the environment (Majestic et al., 2009) due to analytical advances which have made it possible to accurately and precisely measure small variations in stable Fe isotope (^{54}Fe, ^{56}Fe, ^{57}Fe, ^{58}Fe) ratios. Mineral dust has an Fe isotopic composition mirroring that of the crustal rock from which it originated ($+0.07 < \delta^{56}Fe < +0.14$‰; (Beard et al., 2003a, 2003b; Conway et al., 2019), whereas industrial and combustion particles are comparatively lighter ($\sim -3.00 < \delta^{56}Fe < +0.30$‰; (Flament et al., 2008; Kurisu et al., 2016b, 2016a; Mead et al., 2013). This distinction makes Fe isotope ratios a sensitive tool for identifying and distinguishing Fe sources that feed the ocean (Mead et al., 2013). Specifically, low δ^{56}Fe values may be used as a tracer of particles generated by human activities including high-temperature processes (Kurisu et al., 2021; Kurisu and Takahashi, 2019). However, airborne particles are subjected to various physicochemical processes (e.g., acidification, photochemistry, condensation-evaporation) before deposition (Baker and Croot, 2010) and while such 'atmospheric processing' is recognised as enhancing Fe solubility (e.g., (Nickovic et al., 2013; Takahashi et al., 2011; Zhuang et al., 1992), its effect on the Fe isotopic signature and therefore the traceability of the particles remains partially unknown.

Iron is liberated from particulate material mainly by the mechanisms of proton-promoted, ligand-controlled or reductive ligand-promoted dissolution (Chen and Grassian, 2013; Wiederhold et al., 2006). Proton-promoted dissolution of Fe oxides, such as goethite, does not appear to significantly fractionate Fe isotopes during the early stage of dissolution (a few minutes at room temperature; Wiederhold et al., 2006), because it involves protonation of surface sites without breakage of Fe–O bonds. However, studies of Fe-bearing aluminosilicates have shown a preferential release of light Fe isotopes (e.g., ^{54}Fe over ^{56}Fe or ^{57}Fe, or ^{56}Fe over ^{57}Fe or ^{58}Fe) during the early stage of dissolution (Chapman et al., 2009; Kiczka et al., 2010). Similarly, most authors agree that ligand-controlled and reductive ligand-promoted dissolution of aluminosilicates initially (within 60 min) drive an enrichment of the solution in light Fe isotopes (Brantley et al., 2004; Chapman et al., 2009; Kiczka et al., 2010; Mulholland et al., 2021; Wiederhold et al., 2006), due to the formation of Fe-surface complexes with strong chemical bonds, which breaks the weaker Fe–O bonds connecting Fe to the crystal lattice. In this case, the weaker ^{54}Fe–O bonds break more readily than bonds involving heavier Fe isotopes, leading to the preferential solubilisation of ^{54}Fe.

To help fill the knowledge gap of how isotopic fractionation during dissolution processes modifies the Fe signature of atmospheric particles, we previously investigated changes in the soluble Fe isotopic composition during experiments simulating the partial dissolution of pyrogenic particles (industrial ash) in cloud water (Mulholland et al., 2021). The preferential release of ^{54}Fe was observed during early dissolution (after a few minutes), while enrichment of the solution in heavy Fe relative to the initial bulk ash was observed later on (after 60 min). The latter observation was attributed to near-equilibrium conditions reached when Fe-complexes formed in solution have a higher bond energy than the Fe–O bonds existing in the leached solid surface layer. Further evaluation of this effect is necessary as it will occur in parallel with increased Fe dissolution which, in turn, relates to the particles' atmospheric residence time (Rodríguez et al., 2021).

During the particles' atmospheric residence, the release of the heavier ^{56}Fe or ^{57}Fe is inferred to become progressively more dominant over time, due to the ongoing depletion of the leached surface in ^{54}Fe. On a global scale, this means that after long range transport of the particles, the soluble fraction of the atmospheric Fe input to the ocean is expected to have an isotopic composition enriched in heavy Fe isotopes. Conversely, when Fe-bearing particles are deposited near continental source areas, the particle leached surface may not be fully depleted in ^{54}Fe and the soluble fraction of the atmospheric Fe input to the ocean might thus be of lighter Fe isotopic composition than the source particles.

To further improve understanding of processes influencing the Fe isotopic signature of airborne particles during their long-range transport from the source region to the ocean surface, the present study investigates the relationship between Fe dissolution and Fe isotopic fractionation in representative samples of natural and anthropogenic particles. Specifically, we measure the evolution of fractional Fe solubility ($\frac{Fe_{Dissolved}}{Fe_{Total}} \times 100\%$) and Fe isotopic composition over time, in experiments mimicking interaction between mineral dust from a Tunisian desert or industrial ash from an Fe–Mn alloy factory and low pH cloud water, in the presence of oxalic acid (a Fe-complexing organic ligand) and under solar irradiation (UV light), to assess whether these conditions may similarly promote the preferential release of ^{54}Fe and formation of isotopically light secondary particles from both materials.

2. Materials and methods

2.1. Mineral dust sample

A Tunisian desert soil sample was collected from the main dry affluent bed of Oued el Hallouf near Chott El-Djerid (Tunisia; 33°25′38″N, 9°02′08″E). Details on the sampling method and physicochemical characterisation of this particulate material are provided in (Guieu et al., 2010). Briefly, the sample contains 2.3 wt% Fe and consists

of a mixture of quartz, calcite and clays including illite and kaolinite, as confirmed by X-ray powder diffraction analysis (Figure S1 in the Supplementary Information – SI). The particles correspond to the finest fraction (<20 μm) of the collected soil (separated by sieving) and are considered representative of Saharan dust (airborne fraction). The mean size of these particles is ≈ 0.1 μm in diameter (Guieu et al., 2010). The specific surface area was measured by nitrogen gas adsorption according to the Brunauer, Emmett and Teller method (Brunauer et al., 1938) and is equal to 27.2 m^2 g^{-1}.

2.2. Industrial ash sample

Ash particles were collected from an industrial filter of the chimney of the sintering unit (particulate emissions of 32 Mg a^{-1}) of an Fe–Mn alloy manufacturing plant near Dunkirk (northern France; 51°02′N, 2°16′E). Details on the metallurgical plant and physicochemical characterisation of this particulate material have been provided elsewhere (Arndt et al., 2016; Marris et al., 2012, 2013; Mulholland et al., 2021). Briefly, in the firing furnace of the sintering unit, Fe- and Mn-ores are mixed with coal pellets at a temperature of ~400 °C, and then the extraction system collects dust emitted after cooling to 100 °C. These emissions represent a prevailing source of industrial combustion aerosols as sintering units are ubiquitous in the metallurgical industry. The sample contains 6.2 wt% Fe and consists mainly of a mixture of aluminosilicates and Mn- and Fe-oxides (Marris et al., 2013). The material was crushed into a fine powder using an agate mortar and pestle to ensure homogeneity and facilitate acid digestion. The particle size distribution of the powder was measured using a Beckman Coulter LS 13 320 Multi-Wavelength Laser Diffraction Particle Size Analyzer and the mean particle diameter is 0.51 ± 0.14 μm (2 × SD). The specific surface area was measured by nitrogen gas adsorption according to the Brunauer, Emmett and Teller method (Brunauer et al., 1938) and is equal to 3.7 m^2 g^{-1}.

2.3. Mössbauer spectroscopy measurements

2.3.1. Mineral dust

The room-temperature ^{57}Fe Mössbauer spectrum of the mineral dust sample is shown in the SI (Figure S2), with a detailed characterisation of the particles. In summary, three kinds of Fe sites can be differentiated: the most abundant (76 ± 2%) may be associated with goethite, possibly poorly crystallised or Al-substituted. The second (15 ± 2% of Fe sites) is characteristic of hematite α-Fe_2O_3, and the third (9 ± 1% of Fe sites) is similar to those usually observed in Fe(II) silicates such as olivine or cummingtonite.

2.3.2. Industrial ash

A detailed characterisation of the industrial ash particles by Mössbauer spectroscopy was provided by (Mulholland et al., 2021). Briefly, these measurements evidence the presence of α-hematite, magnetite and aluminosilicates internally mixed with Fe- and Mn-oxides. Additional X-ray powder diffraction analyses (Marris et al., 2013) strongly suggest the presence of poorly crystallised manganoferrite nanoparticles in this mixture, potentially representing up to 60 wt% of the Fe-bearing pyrogenic particles.

2.4. Dissolution experiments

As emphasised by (Shi et al., 2012) in their review of atmospheric processing of mineral dust, key parameters influencing atmospheric Fe solubility include organic ligand concentration, pH and dust-to-liquid ratio. Oxalic acid ($H_2C_2O_4$) is used in the present study since this acid and the coupled oxalate ions ($HC_2O_4^-$ and $C_2O_4^{2-}$) are the most widespread organic complexing agents in cloud- and rainwater. They are strong chelating agents with stability constants ranging from 4.2 (Fe(II)) to 9.4 (Fe(III)), considering 1:1 complexes, at 298K (Paris et al., 2011). The action of oxalate anions is typical of a (reductive) ligand-promoted dissolution mechanism and exceeds the effects of most other organic and inorganic anions in cloud- and rainwater (malonate, tartrate, sulphate, acetate, humic compounds) in promoting dissolution of Fe-bearing particles (Chen and Grassian, 2013; Paris and Desboeufs, 2013).

Large variations in cloud and rainwater oxalate concentration, pH and solid-to-liquid ratio have been reported in the literature, depending on the sampling location (Ito and Shi, 2016). used oxalate concentrations ranging from 0 to 30 mM, pH values from 0.9 to 3.1, and dust-to-liquid ratios from 0.06 to 50 g L^{-1}. Here we use intermediate values of 1 mM oxalic acid, pH 2.0 (±0.1) and 250 mg L^{-1} of dust or ash. The pH was adjusted using perchloric acid, as perchlorates have no influence on Fe chelation, unlike oxalates.

(Shi et al., 2012) reported that cloud processing can last from a few hours to several days before the dust is deposited, and (Seinfeld and Pandis, 2006) stated that cloud water condensation and evaporation can occur 5–10 times during this period. Flossmann and Wobrock (2019) suggested a typical lifetime of cloud droplets of a few hours. We therefore ran batch dissolution experiments for 5, 20, 40 and 60 min at room temperature, within 15 mL Savillex© Teflon beakers, under continuous magnetic stirring and irradiation with a solar simulator (Newport© Oriel Solar Simulator). Experiments were conducted in triplicate and a blank run excluding the dust or ash material was also performed for 60 min to assess any procedural Fe contamination. All experiments were performed in a Class 1000 clean air laboratory by personnel equipped with clean room coveralls, clogs and powder-free gloves.

2.5. Soluble Fe concentration analysis

At the end of each experiment, the batch solution containing residual particles was transferred with a pipette into a syringe, filtered through a 0.4 μm cellulose acetate membrane filter, and acidified immediately to 0.5% HNO_3. This filtration protocol is based on the operative definition of soluble Fe including colloidal particles, nanoparticles and aqueous Fe species (Ito and Shi, 2016). In one series of experiments, the filtered leachate was stored in the refrigerator at ~4 °C in the dark until dissolved Fe concentration analysis, within one week. Dissolved Fe concentrations in leachate solutions were analysed by inductively coupled plasma optical emission spectroscopy (ICP-OES - Thermo Instruments ICAP 6300 DUO spectrometer), with standard solution concentrations ranging from 0 to 5000 μg L^{-1} Fe. Operating conditions are reported in the SI (Table S1).

In another series of experiments, the filtered leachate was evaporated at 115 °C and the dried residue was re-dissolved in 1 mL of 6 M HCl for purification prior to Fe isotope analysis (see section 2.6). Reagents were either sub-boiled (HNO_3) or Suprapur® grade ($HClO_4$, HCl, HF). Labware including Savillex© vessels were pre-cleaned for 48 h in 2 M HNO_3 and then 48 h in 0.2 M HNO_3, rinsed three times in ultrapure water (18.2 MΩ cm^{-1}) and dried overnight in a Class 100 laminar flow hood before use.

2.6. Iron isotopic composition analysis

Samples of the original dust and ash material were prepared for Fe isotope analysis by full acid digestion followed by Fe purification by anion exchange chromatography. Purification of sample solutions by anion exchange chromatography was conducted in a Class 100 laminar flow hood located in the Class 1000 clean air laboratory. Acid digestion was conducted at 115 °C for 3 h using a concentrated mixture of 3 mL HNO_3/2 mL HCl/1 mL HF/0.5 mL H_2O_2 in a Savillex© beaker. The liquid was then fully evaporated at 115 °C and the solid residue was re-dissolved in 1 mL of 6 M HCl for subsequent purification, using a Dowex® 1X8 100–200 mesh anion exchange resin, following a modified protocol inspired by (Doucet et al., 2016). Briefly, 1.8 mL of resin was evenly loaded into a Biorad® column and cleaned by the successive passage of H_2O, 6 M HCl, H_2O, 1 M HNO_3, H_2O through the loaded

column and then conditioned in 6 M HCl. The 1 mL of 6 M HCl sample solution containing re-dissolved dry residue from the digested bulk dust or ash or from the evaporated leachate (section 2.5), was then loaded onto the resin and the matrix was rinsed by passing 3 × 10 mL of 6 M HCl through the resin. The Fe was finally eluted by passing 2 × 10 mL of 0.5 M HCl through the resin and collected into a clean Savillex© beaker. This Fe elution fraction was then evaporated at 115 °C. At the start of the isotopic analysis session, the dry residue was re-dissolved in concentrated HNO_3, followed by diluted HNO_3, to obtain a transparent and homogeneous solution containing at least 5 μg Fe for isotope analysis in triplicate. Iron recovery using this protocol has been verified to be >95%. All procedural blanks displayed <1 μg L^{-1} of Fe (i.e. <2% of the total Fe content in the bulk or leachate samples).

Iron isotope analysis was conducted at the Université libre de Bruxelles (Laboratoire G-Time) on a Plasma II multi-collector inductively coupled plasma mass spectrometer (Nu Instruments®), using a standard-sample bracketing method and external normalisation by doping all standards and sample solution with a Ni solution (1000 μg L^{-1}), to correct for instrumental mass bias and drift during the analytical session (de Jong et al., 2007). The Fe isotope data are reported in delta (δ) notation relative to the international Fe isotope standard IRMM-014 (European Commission Institute for Reference Materials and Measurements, Geel, Belgium) as follows:

$$\delta^{56}Fe = \left[\frac{\left(\frac{^{56}Fe}{^{54}Fe}\right) sample}{\left(\frac{^{56}Fe}{^{54}Fe}\right) IRMM} - 1 \right] \times 1000 \quad \text{(Eq. 1)}$$

The extent of isotope fractionation ($\Delta^{56}Fe_{solution\text{-}solid}$) between the two phases in each dissolution experiment was calculated using equations (2) and (3), by comparing the isotopic composition of soluble Fe with the isotopic composition of the initial solid sample:

$$\Delta^{56}Fe_{solution\text{-}dust} = \delta^{56}Fe_{solution} - \delta^{56}Fe_{dust} \quad \text{(Eq. 2)}$$

$$\Delta^{56}Fe_{solution\text{-}ash} = \delta^{56}Fe_{solution} - \delta^{56}Fe_{ash} \quad \text{(Eq. 3)}$$

The Fe isotopic compositions of the initial mineral dust and industrial ash samples have been determined following the protocols described above and are, respectively, $\delta^{56}Fe_{dust} = +0.03 \pm 0.04‰$ (2 × SD) and $\delta^{56}Fe_{ash} = -0.12 \pm 0.08‰$ (2 × SD).

2.7. Kinetic fractionation model

Modelling of the Fe isotope release during dissolution of Fe-bearing particles is based on the kinetic fractionation model developed by (Wiederhold et al., 2006). The model distinguishes Fe atoms according to their atomic mass number and is based on their location in the crystal lattice of the initial bulk mineral, in the reactive surface site (*rss*) pool or in the solution surrounding the mineral. Calculations of the fraction of Fe atoms (ρ, in %) that belong to the *rss* pool, and of the $\delta^{56}Fe_{solution}(\xi)$, which describes the temporal evolution of the Fe isotopic composition in solution, are detailed in the SI.

3. Results and discussion

3.1. Iron solubility

Measured fractional Fe solubilities as a function of time (Fig. 1 and Table S3 in the SI) are consistently two to three times greater for the industrial ash than for the mineral dust.

To account for differences in specific surface area of the dust (27.2 $m^2\ g^{-1}$) and ash (3.7 $m^2\ g^{-1}$) samples, we also report Fe release per unit surface area (in μg m^{-2}) of the dust and ash, as measured in leachate solutions at various experimental time points (Fig. 2). Iron release from the ash is higher by a factor of 40–60 relative to that from the dust. Over

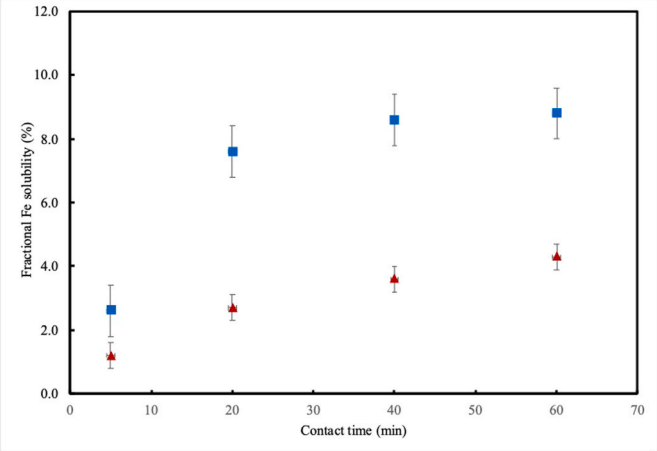

Fig. 1. Fractional Fe solubility as a function of time for mineral dust (red triangles) and industrial ash (blue squares) particles in pH 2 solution containing 1 mM oxalic acid, at a solid-to-liquid ratio of 250 mg L^{-1}, and under irradiation with a solar simulator. Error bars represent ±2 mean standard deviations (three replicates per sample) for X- and Y-axis values. (For interpretation of the references to colour in this figure legend, the reader is referred to the Web version of this article.)

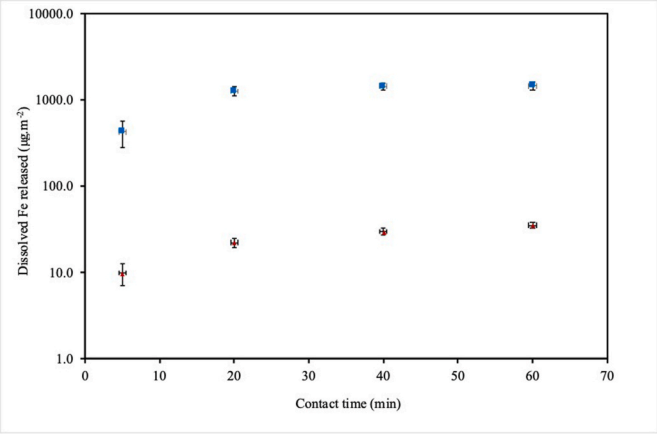

Fig. 2. Surface-area-normalised Fe release as a function of time for mineral dust (red triangles) and industrial ash (blue squares) particles in pH 2 solution containing 1 mM oxalic acid, at a solid-to-liquid ratio of 250 mg L^{-1}, and under irradiation with a solar simulator. Errors bars represent ±2 mean standard deviations (three replicates per sample) for X- and Y-axis values. (For interpretation of the references to colour in this figure legend, the reader is referred to the Web version of this article.)

5 min of dissolution, the dust and ash released up to 10 ± 1 and 427 ± 74 μg Fe m^{-2}, respectively. Over 60 min of dissolution, the dust and ash released up to 35 ± 1 and 1459 ± 106 μg Fe m^{-2}, respectively.

These surface-area-normalised values correspond to fractional Fe solubilities for the dust and ash of 4.2 ± 0.2 and 8.8 ± 0.6%, respectively, over 60 min of dissolution. Clearly, Fe in the ash is much more soluble than in the dust, consistent with numerous studies of Fe solubilities in anthropogenic particles and/or mineral dust (Kurisu et al., 2021; Scanza et al., 2018; Sholkovitz et al., 2012; Takahashi et al., 2013; Winton et al., 2016). However, the estimated fraction of Fe atoms belonging to the *rss* pool is much higher for the dust (ρ = 2.06%; see the SI) than for the ash (ρ = 0.22%; (Mulholland et al., 2021). In other words, dust surfaces expose ~10 times more Fe atoms to solution than ash surfaces, for the same solid mass, even though the dust bulk contains ~2.5 times less Fe than the ash bulk (2.3 wt% vs. 6.2 wt%). However, the soluble Fe released from the ash is always higher than that from the

dust, with a fractional Fe solubility about twice as high after 60 min of dissolution. The contrasting aqueous reactivity of Fe-bearing phases within the two materials is inferred to drive these observed differences in Fe solubility.

The mineral dust particles studied here are composed mainly of quartz, calcite and clays (muscovite, kaolinite; Figure S1 in SI). As underlined by various authors (Marcotte et al., 2020; Paris et al., 2011; Shi et al., 2012), Fe in clays can be present in the interstitial layers between sheets of silica tetrahedra and easily mobilised during aqueous dissolution, and/or trapped in the clay lattice structure (refractory Fe) and hence much less accessible to water molecules, protons and ligands. In any case, the Mössbauer analyses indicate a minor contribution (~10 wt%) of Fe-bearing silicate minerals (olivine, cummingtonite; see section 2.3) to the total Fe content in the dust, and so these minerals are not expected to drive the measured Fe release. Iron in the dust is mainly present in the form of goethite (~75 wt%; see section 2.3), which conforms to previous findings for Saharan soils and dusts (Formenti et al., 2014; Lafon et al., 2006; Scheuvens et al., 2013). The Mössbauer analyses also indicate that goethite essentially occurs as nanoparticles (10–30 nm), in agreement with previous observations of nano-inclusions of Fe oxides aggregated with clays in Saharan soils and dust (Deboudt et al., 2012; Shi et al., 2012). Despite the semi-amorphous crystalline state of goethite, we can assume that the stability of the Fe–O bonds in Fe oxide minerals (dissociation energy >400 kJ mol^{-1} (Marcotte et al., 2020); limits the solubility of goethite nanoparticles present in the dusts.

The industrial ash studied here also contains poorly crystalline Fe oxides, essentially as manganoferrite nanoparticles (~10 nm, i.e. of the same grain size as in the dust), crystallising in a bixbyite type structure (up to 60%; Mulholland et al., 2021). It has been shown that manganese minerals crystallising specifically in a bixbyite type structure have a very high solubility in the presence of oxalate anions (21% at room temperature in a 0.2 M solution of ammonium oxalate, at pH 3, for a bixbyite with a specific surface area of 4 m^2 g^{-1}; (Mendelovici and Sagarzazu, 1991). The differences in Fe solubility observed between the dust and the ash may thus relate to a difference in the nature of the Fe-rich mineral phases within the nanoparticles. As for all industrial combustion units using coal, the ash particles were emitted at the stacks in a SO_2-rich gas mixture, which could lead to the development of low pH (by forming S(VI) species) at the particle surface (Tilgner et al., 2021). It is thus possible that the Fe solubility of the ash was amplified by the existence, within the pores of the material, of an aqueous phase much more acidic than the bulk solution.

3.2. Dissolved iron isotope composition

The Fe isotope compositions ($\delta^{56}Fe$) of the original mineral dust and industrial ash particles are +0.03 ± 0.02 and −0.12 ± 0.04‰, respectively. The $\delta^{56}Fe$ of dissolved Fe in the dust and ash leachate solutions are reported as a function of Fe solubility in Fig. 3 (and Table S3 in the SI).

The Fe isotope fractionation ($\Delta^{56}Fe$) values are reported Fig. 4 and compared with Wiederhold et al. (2006)'s kinetic effect model outputs (see detailed calculations in the SI for mineral dust). Wiederhold et al.'s model uses two fitting parameters: the enrichment factor ε defining the initial fractionation step, and the size of the *rss* pool ρ. In the case of both the dust and ash, a suitable fit is obtained with $\varepsilon = -1.8$‰, expressing an important initial release of ^{54}Fe. The size of the *rss* pool ρ can be calculated using Eq. (1) in (Wiederhold et al., 2006; see the SI). The surface site densities (SSD) of Fe atoms used in the *rss* pool calculations are 6 sites nm^{-2} (Mulholland et al., 2021) for industrial ash and 4.34 sites nm^{-2} for mineral dust (see the SI).

The $\Delta^{56}Fe$ parameter provides a measure of the extent of Fe isotope fractionation between the two phases of interest (solid and solution). A positive value indicates that the solution is enriched in the heavier ^{56}Fe relative to the original solid sample, whereas a negative value indicates that the solution is enriched in the lighter ^{54}Fe relative to the original solid sample. The latter is the case in solutions of both the ash and dust at all Fe solubility points, with the dust consistently showing a greater extent of Fe isotope fractionation than the ash. The observed negative fractionation is consistent with the fact that ligand-controlled and reductive ligand-promoted dissolution processes drive an enrichment of the solution in light Fe (Chapman et al., 2009; Kiczka et al., 2010; Wiederhold et al., 2006). This is due to the formation of strong Fe surface complexes, which result in the weakening of the Fe–O bonds that attach Fe to the crystal lattice. In this case, between Fe–O bonds, the bond involving the lightest isotope is weakest and will break preferentially, thus leading primarily to the release of ^{54}Fe into solution, which we observe experimentally.

Comparison of our $\Delta^{56}Fe$ values with the results of a kinetic fractionation simulation based on the empirical Wiederhold et al. (2006) model (Fig. 4) shows that, while the experimental data are somewhat

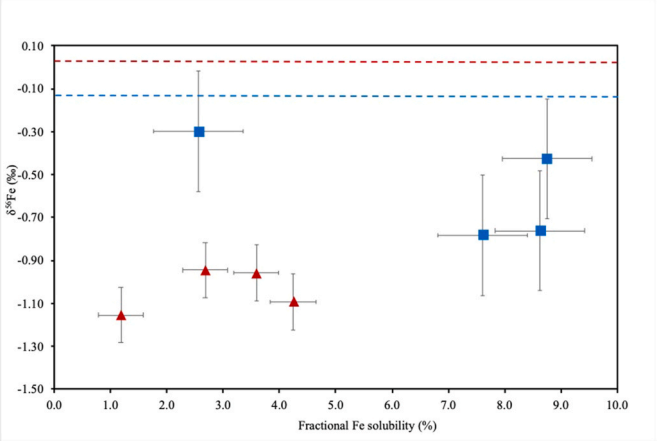

Fig. 3. Dissolved Fe isotope composition ($\delta^{56}Fe$) versus fractional Fe solubility of mineral dust (red triangles) and industrial ash (blue squares). The dashed lines represent the initial isotope compositions of the dust (red line) and ash (blue line) (see text). Error bars represent ±2 mean standard deviations (three replicates per sample) for X- and Y-axis values. (For interpretation of the references to colour in this figure legend, the reader is referred to the Web version of this article.)

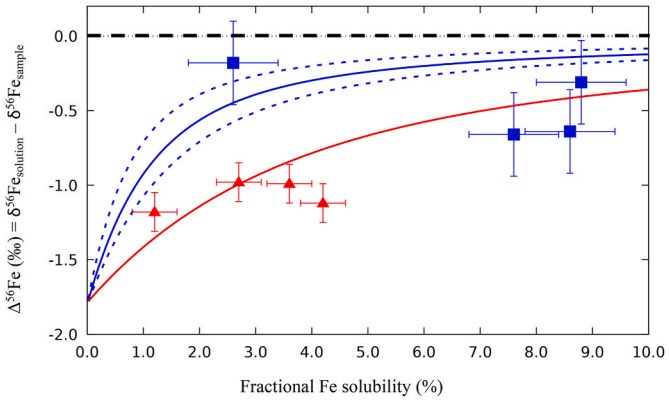

Fig. 4. ^{56}Fe fractionation ($\Delta^{56}Fe = \delta^{56}Fe_{solution} - \delta^{56}Fe_{solid}$; see text) for mineral dust (red triangles) and industrial ash (blue squares) particles versus fractional Fe solubility. The dashed black line corresponds to $\Delta^{56}Fe = 0$. Error bars represent ±2 mean standard deviations (three replicates per sample) for X- and Y-axis values. Also shown are the kinetic fractionation model fit curves obtained for the dust (solid red line; $\varepsilon = -1.8$‰ and SSD = 4.34 sites nm^{-2}) and for the ash (solid blue line; $\varepsilon = -1.8$‰ and SSD = 6 sites nm^{-2}). The dashed blue lines indicate SSD = 4 [upper curve] and SSD = 8 [lower curve] sites nm^{-2}, respectively. (For interpretation of the references to colour in this figure legend, the reader is referred to the Web version of this article.)

dispersed, the shape of the kinetic fractionation phenomenon is reasonably described taking into account experimental uncertainties, in terms of measurement of both Fe solubility and δ^{56}Fe in solution. Considering the trend illustrated by the curve from the empirical model (Fig. 4), the δ^{56}Fe of the dissolved Fe appears to gradually approach that of the Fe in the original solid sample. This is consistent with the ongoing depletion of ^{54}Fe in the surface reactive layer of the solid, progressively leading to the release of the heavier isotopes into solution, with the difference between the $\delta^{56}Fe_{solution}$ and the $\delta^{56}Fe_{solid}$ tending towards zero. This probably corresponds to the attainment of an equilibrium between the solid and the solution, as the Δ^{56}Fe of zero is coincident with the concentration of soluble Fe no longer changing, either for the ash or for the dust (Fig. 2). The progressive achievement of this equilibrium is consistent with a ligand-controlled dissolution process, i.e. an initial enrichment of the solution in light Fe, followed by the release of the heavier isotopes into solution when the surface reactive layer of the solid becomes depleted in light Fe.

3.3. Surface iron complexation mechanisms and isotope fractionation

Numerous literature studies report the dissolution kinetics of Fe-(oxyhydr)oxides in the presence of ligands such as oxalic acid and its pH-dependent anionic forms ($HC_2O_4^-$ and $C_2O_4^{2-}$). These include goethite in the dust sample studied here and hematite present in the ash sample. Although hematite is not the dominant mineral in the pyrogenic particles, it may be appropriate to refer also to the work on α-hematite for comparison with the findings for goethite. Generally speaking, with a bidentate ligand such as oxalic acid, a surface chelate called an "inner-sphere complex" is formed. This could be the first step in the dissolution process, followed by the release of the chelated Fe(III) ion, before a final step of surface site restoration by proton adsorption (Cornell and Schwertmann, 2003). This mechanism facilitates the dissolution of Fe oxides because the action of the ligand increases the electron density within the coordination sphere of Fe (vacant *d*-orbitals of Fe(III), as a Lewis acid), thereby increasing the electron density on the O-atom bonded to Fe(III) within the crystal lattice, which will then facilitate the restoration of the surface site by protonation after detachment of the chelated Fe(III) (Stumm, 1992). It may therefore be relevant to consider the number of chelated surface sites to explain the differences between the dust and ash Fe solubilities. The proportion of surface Fe atoms chelated by oxalic acid can be approximated using the Langmuir isotherm model (Duckworth and Martin, 2001), following equation (4):

$$\theta = \frac{K[A]}{1 + K[A]} \quad \text{(Eq. 4)}$$

Where θ is the fractional surface coverage ($0 < \theta < 1$), K is the Langmuir binding constant between the surface and the ligand (oxalic acid) in M^{-1}, and $[A]$ is the aqueous ligand concentration (1 mM). With oxalic acid as a ligand, reported K values for hematite – as a proxy for ash (Duckworth and Martin, 2001) and goethite – as a proxy for dust (Mesuere and Fish, 1992) are 30 000 ± 3000 and 4.8 ± 0.2 × 10^{11}, respectively. Using these values in equation (4), we obtain a fractional surface coverage θ of ~0.968 for hematite and >0.999 for goethite, respectively. These results must be viewed with caution since α-Fe_2O_3 is not the main mineral phase in the ash, even if the available data for hematite constitutes an interesting basis for comparison in the absence of data for Fe_3O_4 and $FeMnO_3$, the other phases present in the ash (Mulholland et al., 2021). These results suggest that, if the formation of the inner-sphere complex is the driving force of the dissolution process, the Fe solubility at final equilibrium (contact time ~60 min) should be higher for the dust than for the ash. However, (Simanova et al., 2011) observed that during the dissolution of goethite particles, in the presence of oxalate ions, two types of surface complexes were formed: "outer-sphere complexes" which are the main species at the beginning of dissolution, and inner-sphere complexes which become the main surface complexes as the dissolved Fe concentration increases. These are type A ternary surface complexes (i.e. {surface site}-OFe-Ligand; (Schindler, 1990)) resulting from the re-adsorption of Fe(III), which limits the quantity of Fe released into solution. We hypothesise that it is this dissolution-re-adsorption mechanism that limits the solubility of Fe in dust in due course, the phenomenon being probably less significant for the ash because the proportion of surface Fe atoms accessible to ligands is slightly lower. By blocking surface sites available for further dissolution, these re-adsorption phenomena prevent the release of Fe into solution. In this respect, (Simanova et al., 2011) noted that these A-type complexes adsorb on the most stable surface sites which, apart from any consideration of high-energy crystalline faces or defect sites, could be sites where Fe–O surface bonds are energetically stronger. Thus, this could prevent the release of heavy isotopes in solution and maintain a relative ^{54}Fe enrichment in solution (negative fractionation), which we observe for both types of particles but with a more pronounced effect for dust.

4. Conclusion

Current geochemical models of Fe-bearing particle deposition to the ocean surface typically consider four main parameters controlling the amount of soluble Fe deposited:

- the pH dependence of proton-promoted dissolution during atmospheric transport
- the redox reactions between Fe(II) and Fe(III), enhanced by photochemistry
- the nature and concentration of complexing agents (ligand-controlled dissolution)
- the nature and amount of Fe-containing minerals

Our results show that in the presence of a very common complexing agent in cloud water (oxalic acid), the amount of Fe released per unit surface area from particles representative of high-temperature combustion processes (industrial ash: ~1460 μg Fe m^{-2}) is about 40 times higher than that released by desert dust (~35 μg Fe m^{-2}), after 60 min of contact with solution. This production of dissolved Fe is accompanied by an isotopic fractionation leading to the preferential release of ^{54}Fe in solution over 1 h. Isotopic fractionation is more significant in the mineral dust than the industrial ash, which we infer to relate to the re-adsorption of A-type ternary complexes on the most stable surface sites of particles, i.e. sites where Fe–O surface bonds are energetically stronger (^{56}Fe–O and ^{57}Fe–O surface sites). This phenomenon could counteract the liberation of heavy Fe isotopes, after the initial release of the lighter isotope, and maintain a relative ^{54}Fe enrichment in solution.

Accurate estimation of the amount of soluble Fe delivered to the ocean surface is a prerequisite for understanding the oceanic Fe cycle and the limitation of marine primary production in some areas of the world oceans (Ito et al., 2021). Iron isotopes have been used as a tool for several decades to investigate the oceanic Fe cycle, but more recently to validate atmospheric chemistry-transport models that address the magnitude of soluble Fe input to different regions of the ocean (Kurisu et al., 2021). The effective use of Fe isotope tracing in model validation requires an understanding of the fractionation phenomena occurring in the troposphere, especially during the incorporation of Fe-bearing particles into cloud droplets. The present study is a first step in the analysis of Fe isotopic fractionation occurring during so-called cloud processing of aerosol particles. A more refined description can be achieved by additional laboratory studies of Fe isotopic fractionation under more atmospherically relevant conditions, taking into account a wider range of temperatures (e.g. representative of high-altitude clouds) and solid-to-liquid ratios.

Author contributions

Elena C. Maters: Investigation, Methodology, Validation, Writing (Original Draft); **Daniel S. Mulholland:** Validation, Writing (Review & Editing); **Pascal Flament**: Conceptualization, Resources, Formal analysis, Writing (Original Draft), Supervision, Funding acquisition; **Jeroen de Jong:** Investigation, Validation, Formal analysis, Writing (Review & Editing); **Nadine Mattielli:** Validation, Formal analysis, Writing (Review & Editing), Funding acquisition; **Karine Deboudt:** Resources, Visualization, Funding acquisition, Writing (Review & Editing); **Guillaume Dhont**: Software, Formal analysis, Data curation, Writing (Review & Editing); **Eugène Bychkov**: Validation, Formal analysis, Visualization, Writing (Original Draft).

Declaration of competing interest

The authors declare that they have no known competing financial interests or personal relationships that could have appeared to influence the work reported in this paper.

Acknowledgements

LPCA acknowledge financial support from the CaPPA (Chemical and Physical Properties of the Atmosphere) project funded by the French National Research Agency (ANR), through the PIA (Programme d'Investissement d'Avenir) under contract ANR-11-LABX-0005-01, and from the CPER project CLIMIBIO funded by the French Ministry of Higher Education and Research, the CNRS, the Regional Council "Hauts-de-France" and the European Regional Development Fund (ERDF). The authors express special thanks to Karine Desboeufs (LISA-UPEC, UMR CNRS 7583, France) for providing the Tunisian soil sample used in this study and Dominique Weis and Laure Aimoz (Earth & Ocean Science Dept. – UBC, Vancouver) for the X-ray analysis of this sample. The authors also thank Dorothée Dewaele for supporting Fe concentration measurements and Wendy Debouge for valuable training and advice on Fe separation and purification for isotope analysis. ECM currently benefits from an Early Career Fellowship funded jointly by the Leverhulme Trust and Isaac Newton Trust.

Appendix A. Supplementary data

Supplementary data to this article can be found online at https://doi.org/10.1016/j.chemosphere.2022.134472.

References

Arndt, J., Deboudt, K., Anderson, A., Blondel, A., Eliet, S., Flament, P., Fourmentin, M., Healy, R.M., Savary, V., Setyan, A., Wenger, J.C., 2016. Scanning electron microscopy-energy dispersive X-ray spectrometry (SEM-EDX) and aerosol time-of-flight mass spectrometry (ATOFMS) single particle analysis of metallurgy plant emissions. Environ. Pollut. 210, 9–17. https://doi.org/10.1016/j.envpol.2015.11.019.

Baker, A.R., Croot, P.L., 2010. Atmospheric and marine controls on aerosol iron solubility in seawater. Mar. Chem. 120, 4–13. https://doi.org/10.1016/j.marchem.2008.09.003.

Baker, A.R., Landing, W.M., Bucciarelli, E., Cheize, M., Fietz, S., Hayes, C.T., Kadko, D., Morton, P.L., Rogan, N., Sarthou, G., Shelley, R.U., Shi, Z., Shiller, A., van Hulten, M. M.P., 2016. Trace element and isotope deposition across the air–sea interface: progress and research needs. Philos. Trans. R. Soc. Math. Phys. Eng. Sci. 374, 20160190. https://doi.org/10.1098/rsta.2016.0190.

Beard, B.L., Johnson, C.M., Skulan, J.L., Nealson, K.H., Cox, L., Sun, H., 2003a. Application of Fe isotopes to tracing the geochemical and biological cycling of Fe. Chem. Geol. 195, 87–117. https://doi.org/10.1016/S0009-2541(02)00390-X.

Beard, B.L., Johnson, C.M., Von Damm, K.L., Poulson, R.L., 2003b. Iron isotope constraints on Fe cycling and mass balance in oxygenated Earth oceans. Geology 31, 629. https://doi.org/10.1130/0091-7613(2003)031<0629:IICOFC>2.0.CO;2.

Boyd, P.W., Ellwood, M.J., 2010. The biogeochemical cycle of iron in the ocean. Nat. Geosci. 3, 675–682. https://doi.org/10.1038/ngeo964.

Brantley, S.L., Liermann, L.J., Guynn, R.L., Anbar, A., Icopini, G.A., Barling, J., 2004. Fe isotopic fractionation during mineral dissolution with and without bacteria. Geochem. Cosmochim. Acta 68, 3189–3204. https://doi.org/10.1016/j.gca.2004.01.023.

Brunauer, S., Emmet, P.H., Teller, E., 1938. Adsorption of gases in multimoleculer layers. J. Am. Chem. Soc. 60, 309–319.

Chapman, J.B., Weiss, D.J., Shan, Y., Lemburger, M., 2009. Iron isotope fractionation during leaching of granite and basalt by hydrochloric and oxalic acids. Geochem. Cosmochim. Acta 73, 1312–1324. https://doi.org/10.1016/j.gca.2008.11.037.

Chen, H., Grassian, V.H., 2013. Iron dissolution of dust source materials during simulated acidic processing: the effect of sulfuric, acetic, and oxalic acids. Environ. Sci. Technol. 47, 10312–10321. https://doi.org/10.1021/es401285s.

Chen, T., Li, W., Guo, B., Liu, R., Li, G., Zhao, L., Ji, J., 2020. Reactive iron isotope signatures of the East Asian dust particles: implications for iron cycling in the deep North Pacific. Chem. Geol. 531, 119342. https://doi.org/10.1016/j.chemgeo.2019.119342.

Conway, T.M., Hamilton, D.S., Shelley, R.U., Aguilar-Islas, A.M., Landing, W.M., Mahowald, N.M., John, S.G., 2019. Tracing and constraining anthropogenic aerosol iron fluxes to the North Atlantic Ocean using iron isotopes. Nat. Commun. 10, 2628. https://doi.org/10.1038/s41467-019-10457-w.

Conway, T.M., John, S.G., 2014. Quantification of dissolved iron sources to the North atlantic ocean. Nature 511, 212–215. https://doi.org/10.1038/nature13482.

Cornell, R.M., Schwertmann, U., 2003. The Iron Oxides, Second. Wiley-VCH Verlag GmbH, Weinheim.

de Baar, H.J.W., 2005. Synthesis of iron fertilization experiments: from the iron age in the age of enlightenment. J. Geophys. Res. 110, C09S16. https://doi.org/10.1029/2004JC002601.

de Jong, J., Schoemann, V., Tison, J.-L., Becquevort, S., Masson, F., Lannuzel, D., Petit, J., Chou, L., Weis, D., Mattielli, N., 2007. Precise measurement of Fe isotopes in marine samples by multi-collector inductively coupled plasma mass spectrometry (MC-ICP-MS). Anal. Chim. Acta 589, 105–119. https://doi.org/10.1016/j.aca.2007.02.055.

Deboudt, K., Gloter, A., Mussi, A., Flament, P., 2012. Red-ox speciation and mixing state of iron in individual African dust particles: Fe in African dust particles. J. Geophys. Res. Atmos. 117 https://doi.org/10.1029/2011JD017298 n/a-n/a.

Doucet, L.S., Mattielli, N., Ionov, D.A., Debouge, W., Golovin, A.V., 2016. Zn isotopic heterogeneity in the mantle: a melting control? Earth Planet Sci. Lett. 451, 232–240. https://doi.org/10.1016/j.epsl.2016.06.040.

Duce, R.A., Tindale, N.W., 1991. Atmospheric transport of iron ans its deposition in the ocean. Limnol. Oceanogr. 36, 1715–1726.

Duckworth, O.W., Martin, S.T., 2001. Surface complexation and dissolution of hematite by C 1 -C 6 dicarboxylic acids at pH = 5.0. Geochem. Cosmochim. Acta 65, 4289–4301. https://doi.org/10.1016/S0016-7037(01)00696-2.

Flament, P., Mattielli, N., Aimoz, L., Choël, M., Deboudt, K., Jong, J. de, Rimetz-Planchon, J., Weis, D., 2008. Iron isotopic fractionation in industrial emissions and urban aerosols. Chemosphere 73, 1793–1798. https://doi.org/10.1016/j.chemosphere.2008.08.042.

Flossmann, A.I., Wobrock, W., 2019. Cloud processing of aerosol particles in marine stratocumulus clouds. Atmosphere 10, 520. https://doi.org/10.3390/atmos10090520.

Formenti, P., Caquineau, S., Chevaillier, S., Klaver, A., Desboeufs, K., Rajot, J.L., Belin, S., Briois, V., 2014. Dominance of goethite over hematite in iron oxides of mineral dust from Western Africa: quantitative partitioning by X-ray absorption spectroscopy. J. Geophys. Res. Atmos. 119 (12) https://doi.org/10.1002/2014JD021668, 740-12,754.

Guieu, C., Dulac, F., Desboeufs, K., Wagener, T., Pulido-Villena, E., Grisoni, J.-M., Louis, F., Ridame, C., Blain, S., Brunet, C., Bon Nguyen, E., Tran, S., Labiadh, M., Dominici, J.-M., 2010. Large clean mesocosms and simulated dust deposition: a new methodology to investigate responses of marine oligotrophic ecosystems to atmospheric inputs. Biogeosciences 7, 2765–2784. https://doi.org/10.5194/bg-7-2765-2010.

Hutchins, D.A., Bruland, K.W., 1998. Iron-limited diatom growth and Si:N ratios in a coastal upwelling regime. Nature 393, 561–564.

Ito, A., Myriokefalitakis, S., Kanakidou, M., Mahowald, N.M., Scanza, R.A., Hamilton, D. S., Baker, A.R., Jickells, T., Sarin, M., Bikkina, S., Gao, Y., Shelley, R.U., Buck, C.S., Landing, W.M., Bowie, A.R., Perron, M.M.G., Guieu, C., Meskhidze, N., Johnson, M. S., Feng, Y., Kok, J.F., Nenes, A., Duce, R.A., 2019. Pyrogenic iron: the missing link to high iron solubility in aerosols. Sci. Adv. 5, eaau7671. https://doi.org/10.1126/sciadv.aau7671.

Ito, A., Shi, Z., 2016. Delivery of anthropogenic bioavailable iron from mineral dust and combustion aerosols to the ocean. Atmos. Chem. Phys. 16, 85–99. https://doi.org/10.5194/acp-16-85-2016.

Ito, A., Ye, Y., Baldo, C., Shi, Z., 2021. Ocean fertilization by pyrogenic aerosol iron. Npj Clim. Atmospheric Sci. 4, 30. https://doi.org/10.1038/s41612-021-00185-8.

Kiczka, M., Wiederhold, J.G., Frommer, J., Kraemer, S.M., Bourdon, B., Kretzschmar, R., 2010. Iron isotope fractionation during proton- and ligand-promoted dissolution of primary phyllosilicates. Geochem. Cosmochim. Acta 74, 3112–3128. https://doi.org/10.1016/j.gca.2010.02.018.

Kurisu, M., Sakata, K., Miyamoto, C., Takaku, Y., Iizuka, T., Takahashi, Y., 2016a. Variation of iron isotope ratios in anthropogenic materials emitted through combustion processes. Chem. Lett. 45, 970–972. https://doi.org/10.1246/cl.160451.

Kurisu, M., Sakata, K., Uematsu, M., Ito, A., Takahashi, Y., 2021. Contribution of combustion Fe in marine aerosols over the northwestern Pacific estimated by Fe stable isotope ratios. Atmos. Chem. Phys. 21, 16027–16050. https://doi.org/10.5194/acp-21-16027-2021.

Kurisu, M., Takahashi, Y., Iizuka, T., Uematsu, M., 2016b. Very low isotope ratio of iron in fine aerosols related to its contribution to the surface ocean: iron Isotope in Anthropogenic Aerosols. J. Geophys. Res. Atmos. 121 (11) https://doi.org/10.1002/2016JD024957, 119-11,136.

Lafon, S., Sokolik, I.N., Rajot, J.L., Caquineau, S., Gaudichet, A., 2006. Characterization of iron oxides in mineral dust aerosols: implications for light absorption. J. Geophys. Res. 111, D21207. https://doi.org/10.1029/2005JD007016.

Lam, P.J., Bishop, J.K.B., 2008. The continental margin is a key source of iron to the HNLC North Pacific Ocean: continental margin and the North Pacific. Geophys. Res. Lett. 35 https://doi.org/10.1029/2008GL033294 n/a-n/a.

Luo, C., Mahowald, N., Bond, T., Chuang, P.Y., Artaxo, P., Siefert, R., Chen, Y., Schauer, J., 2008. Combustion iron distribution and deposition: combustion iron. Global Biogeochem. Cycles 22. https://doi.org/10.1029/2007GB002964 n/a-n/a.

Mahowald, N.M., Engelstaedter, S., Luo, C., Sealy, A., Artaxo, P., Benitez-Nelson, C., Bonnet, S., Chen, Y., Chuang, P.Y., Cohen, D.D., Dulac, F., Herut, B., Johansen, A.M., Kubilay, N., Losno, R., Maenhaut, W., Paytan, A., Prospero, J.M., Shank, L.M., Siefert, R.L., 2009. Atmospheric iron deposition: global distribution, variability, and human perturbations. Ann. Rev. Mar. Sci 1, 245–278. https://doi.org/10.1146/annurev.marine.010908.163727.

Majestic, B.J., Anbar, A.D., Herckes, P., 2009. Stable isotopes as a tool to apportion atmospheric iron. Environ. Sci. Technol. 43, 4327–4333. https://doi.org/10.1021/es900023w.

Marcotte, A.R., Anbar, A.D., Majestic, B.J., Herckes, P., 2020. Mineral dust and iron solubility: effects of composition, particle size, and surface area. Atmosphere 11, 533. https://doi.org/10.3390/atmos11050533.

Marris, H., Deboudt, K., Augustin, P., Flament, P., Blond, F., Fiani, E., Fourmentin, M., Delbarre, H., 2012. Fast changes in chemical composition and size distribution of fine particles during the near-field transport of industrial plumes. Sci. Total Environ. 427, 126–138. https://doi.org/10.1016/j.scitotenv.2012.03.068. –428.

Marris, H., Deboudt, K., Flament, P., Grobéty, B., Gieré, R., 2013. Fe and Mn oxidation states by TEM-EELS in fine-particle emissions from a Fe–Mn alloy making plant. Environ. Sci. Technol. 47, 10832–10840. https://doi.org/10.1021/es400368s.

Martin, J.H., Fitzwater, S.E., 1988. Iron deficiency limits phytoplankton growth in the north-east Pacific subartic. Nature 331, 341–343.

Mead, C., Herckes, P., Majestic, B.J., Anbar, A.D., 2013. Source apportionment of aerosol iron in the marine environment using iron isotope analysis: sourcing aerosol Fe by isotope analysis. Geophys. Res. Lett. 40, 5722–5727. https://doi.org/10.1002/2013GL057713.

Mendelovici, E., Sagarzazu, A., 1991. Characteristics of products from the acid ammonium oxalate treatment of manganese minerals. Clay Clay Miner. 39, 264–269.

Mesuere, K., Fish, W., 1992. Chromate and oxalate adsorption on goethite. 1. Calibration of surface complexation models. Environ. Sci. Technol. 26, 2357–2364. https://doi.org/10.1021/es00036a004.

Morel, F.M.M., Hudson, R.J.M., Price, N.M., 1991. Limitation of productivity by trace metals in the sea. Limnol. Oceanogr. 36, 1742–1755.

Mulholland, D.S., Flament, P., de Jong, J., Mattielli, N., Deboudt, K., Dhont, G., Bychkov, E., 2021. In-cloud processing as a possible source of isotopically light iron from anthropogenic aerosols: new insights from a laboratory study. Atmos. Environ. 259, 118505. https://doi.org/10.1016/j.atmosenv.2021.118505.

Nickovic, S., Vukovic, A., Vujadinovic, M., 2013. Atmospheric processing of iron carried by mineral dust. Atmos. Chem. Phys. 13, 9169–9181. https://doi.org/10.5194/acp-13-9169-2013.

Paris, R., Desboeufs, K.V., Journet, E., 2011. Variability of dust iron solubility in atmospheric waters: Investigation of the role of oxalate organic complexation. Atmos. Environ. 45, 6510–6517. https://doi.org/10.1016/j.atmosenv.2011.08.068.

Rodríguez, S., Prospero, J.M., López-Darias, J., García-Alvarez, M.-I., Zuidema, P., Nava, S., Lucarelli, F., Gaston, C.J., Galindo, L., Sosa, E., 2021. Tracking the changes of iron solubility and air pollutants traces as African dust transits the Atlantic in the Saharan dust outbreaks. Atmos. Environ. 246, 118092. https://doi.org/10.1016/j.atmosenv.2020.118092.

Scanza, R.A., Hamilton, D.S., Perez Garcia-Pando, C., Buck, C., Baker, A., Mahowald, N. M., 2018. Atmospheric processing of iron in mineral and combustion aerosols: development of an intermediate-complexity mechanism suitable for Earth system models. Atmos. Chem. Phys. 18, 14175–14196. https://doi.org/10.5194/acp-18-14175-2018.

Scheuvens, D., Schütz, L., Kandler, K., Ebert, M., Weinbruch, S., 2013. Bulk composition of northern African dust and its source sediments — a compilation. Earth Sci. Rev. 116, 170–194. https://doi.org/10.1016/j.earscirev.2012.08.005.

Schindler, P.W., 1990. Co-adsorption of metal ions and organic ligands : formation of ternary surface complexes. In: Mineral-water Interface Geochemistry. Mineralogical Society of America, Washington, DC, pp. 281–307.

Sedwick, P.N., Sholkovitz, E.R., Church, T.M., 2007. Impact of anthropogenic combustion emissions on the fractional solubility of aerosol iron: evidence from the Sargasso Sea: fractional solubility of aerosol iron. Geochem. Geophys. Geosystems 8. https://doi.org/10.1029/2007GC001586 n/a-n/a.

Seinfeld, J.H., Pandis, S.N., 2006. Atmospheric Chemistry and Physics from Air Pollution to Climate Change, Second. John Wiley & Sons Inc., New York.

Shi, Z., Krom, M.D., Jickells, T.D., Bonneville, S., Carslaw, K.S., Mihalopoulos, N., Baker, A.R., Benning, L.G., 2012. Impacts on iron solubility in the mineral dust by processes in the source region and the atmosphere: a review. Aeolian Res 5, 21–42. https://doi.org/10.1016/j.aeolia.2012.03.001.

Sholkovitz, E.R., Sedwick, P.N., Church, T.M., 2009. Influence of anthropogenic combustion emissions on the deposition of soluble aerosol iron to the ocean: empirical estimates for island sites in the North Atlantic. Geochem. Cosmochim. Acta 73, 3981–4003. https://doi.org/10.1016/j.gca.2009.04.029.

Sholkovitz, E.R., Sedwick, P.N., Church, T.M., Baker, A.R., Powell, C.F., 2012. Fractional solubility of aerosol iron: synthesis of a global-scale data set. Geochem. Cosmochim. Acta 89, 173–189. https://doi.org/10.1016/j.gca.2012.04.022.

Simanova, A.A., Loring, J.S., Persson, P., 2011. formation of ternary metal-oxalate surface complexes on α-FeOOH particles. J. Phys. Chem. C 115, 21191–21198. https://doi.org/10.1021/jp2058707.

Stumm, W., 1992. Chemistry of the Solid-Water Interface, First. ed. John Wiley & Sons Inc., New York.

Tagliabue, A., Bopp, L., Dutay, J.-C., Bowie, A.R., Chever, F., Jean-Baptiste, P., Bucciarelli, E., Lannuzel, D., Remenyi, T., Sarthou, G., Aumont, O., Gehlen, M., Jeandel, C., 2010. Hydrothermal contribution to the oceanic dissolved iron inventory. Nat. Geosci. 3, 252–256. https://doi.org/10.1038/ngeo818.

Tagliabue, A., Bowie, A.R., Boyd, P.W., Buck, K.N., Johnson, K.S., Saito, M.A., 2017. The integral role of iron in ocean biogeochemistry. Nature 543, 51–59. https://doi.org/10.1038/nature21058.

Takahashi, Y., Furukawa, T., Kanai, Y., Uematsu, M., Zheng, G., Marcus, M.A., 2013. Seasonal changes in Fe species and soluble Fe concentration in the atmosphere in the Northwest Pacific region based on the analysis of aerosols collected in Tsukuba, Japan. Atmos. Chem. Phys. 13, 7695–7710. https://doi.org/10.5194/acp-13-7695-2013.

Takahashi, Y., Higashi, M., Furukawa, T., Mitsunobu, S., 2011. Change of iron species and iron solubility in Asian dust during the long-range transport from western China to Japan. Atmos. Chem. Phys. 11, 11237–11252. https://doi.org/10.5194/acp-11-11237-2011.

Tilgner, A., Schaefer, T., Alexander, B., Barth, M., Collett Jr., J.L., Fahey, K.M., Nenes, A., Pye, H.O.T., Herrmann, H., McNeill, V.F., 2021. Acidity and the multiphase chemistry of atmospheric aqueous particles and clouds. Atmos. Chem. Phys. 21, 13483–13536. https://doi.org/10.5194/acp-21-13483-2021.

Wang, F.J., Chen, Y., Guo, Z.G., Gao, H.W., Mackey, K.R., Yao, X.H., Zhuang, G.S., Paytan, A., 2017. Combined effects of iron and copper from atmospheric dry deposition on ocean productivity. Geophys. Res. Lett. 44, 2546–2555. https://doi.org/10.1002/2016GL072349.

Wiederhold, J.G., Kraemer, S.M., Teutsch, N., Borer, P.M., Halliday, A.N., Kretzschmar, R., 2006. Iron isotope fractionation during proton-promoted, ligand-controlled, and reductive dissolution of Goethite. Environ. Sci. Technol. 40, 3787–3793.

Winton, V.H.L., Edwards, R., Bowie, A.R., Keywood, M., Williams, A.G., Chambers, S.D., Selleck, P.W., Desservettaz, M., Mallet, M.D., Paton-Walsh, C., 2016. Dry season aerosol iron solubility in tropical northern Australia. Atmos. Chem. Phys. 16, 12829–12848. https://doi.org/10.5194/acp-16-12829-2016.

Zhuang, G., Yi, Z., Duce, R.A., Brown, P.R., 1992. Chemistry of iron in marine aerosols. Global Biogeochem. Cycles 6, 161–173.